Ma, X.; Blawert, C.; Hoeche, D.; Zheludkevich, M.L.; Kainer, K.U.:

Investigation of electrode distance impact on PEO coating formation assisted by simulation

In: Applied Surface Science (2016) Elsevier

DOI: 10.1016/j.apsusc.2016.01.030

Investigation of electrode distance impact on PEO coating properties assisted by simulation

Xun Ma *, Carsten Blawert, Daniel Höche, Mikhail L. Zheludkevich, Karl U. Kainer

Helmholtz-Zentrum Geesthacht Zentrum für Material-und Küstenforschung GmbH, Institute of Materials Research, Max-Plank-Str. 1, 21502 Geesthacht, Germany

Abstract:

To better understand the influence of electrode distance between anode and cathode during plasma electrolytic oxidation (PEO) process, present study investigates its impact on the coating properties through experiments and assisted simulation. Firstly a model was built to simulate the effect of electrode distance on anode current using COMSOL software package. Complementary, PEO coatings were fabricated on AM50 magnesium alloy in alkaline electrolyte with different electrode distances under constant voltage by a DC power supply. Coating morphology, phase composition and coating thickness were studied at each electrode distance. Through combining the simulation and experiment results, the interaction between electrode distance and coating features is explored. It is demonstrated that under constant voltage mode, PEO coating features on both front and back sides of magnesium samples are affected by electrode distances, which ascribes to the changed current distribution in the bath and related average current density on the surfaces induced by electrode distances.

Key words: PEO; electrode distance; simulation; current; magnesium;

1. Introduction

PEO is an anodizing surface engineering technology used to fabricate ceramic-like coatings on light metals (Mg, Al and Ti) and their alloys [1-3]. This technology requires a power supply to provide high voltage that can maintain the dielectric breakdown of the oxide film growing on the surface of a metal anode, and mainly alkaline electrolytes based on silicate, phosphate and/or aluminate [4-5]. Since the investment costs of the equipment are relatively low and the electrolytes are without any pollutant compounds, PEO is considered to be one of the most cost-effective and environmentally friendly ways to provide enhanced corrosion protection, wear resistance, biomimetic and thermal barrier properties for light metals [6].

When the supplied voltage above the breakdown potential applied, PEO process in constant current mode can be identified as four stages distinguished by the discharge characteristics. The early stage involves the rapid electrochemical formation of an initial insulating oxide film, accompanied by rapid rise of the cell potential till the so called breakdown potential is obtained [7]. And then PEO steps into the second stage, where numerous sparks move rapidly over the whole sample surface area. The rate of the voltage change decreases which indicates the start of the breakdown of the oxide layer, the increase of temperature and subsequent melting of the substrate metal [8]. The third Stage is characterized by larger but slower moving discharges and the growing oxide layer. In stage four, less frequent discharges appear as relatively large and long lasting sparks due to the thicker coating causing more difficulty in the initiation of such discharges [9]. The coatings formed by PEO on magnesium alloys are typically thick (ranges from tens to hundreds of microns [10]), porous, hard and well-adherent to the substrate [11]. The frictional, corrosive, electrical and thermal properties of these coatings have generated interest for their use in mechanical, aerospace and engineering equipment components, as well as for biomedical devices [12,13]. PEO process is known to be complex due to the involvement of anodic oxidation, dielectric breakdown, gas evolution, cathodic breakdown and thermo-chemical driven plasma expansion [14]. For decades various

researchers have investigated the formation mechanisms and influence factors of PEO to optimize the treatment parameters for the purpose of improving the coating characteristics. Parameters such as electrolyte compositions, substrate materials, the electric parameters (mainly current mode and current density), and process time were studied their impact on coating morphologies and properties.

Among all the factors, current density was considered as the principal parameter [15,16], but the electrode distance between anode and cathode was deemed negligible and only few papers studied its influence. Melhem et al. [17] suggested that distance may be influent, depending on the process conditions, and should nonetheless be taken into account. Also, Wei et al. [18] demonstrated that the distance between anode and cathode affected the anode current and the oxidation efficiency. Therefore, the distance effect has to be considered. Thus, in this paper, PEO coatings were produced with different electrode distances ranging from 10 mm to 240 mm under constant voltage. The coating features including phase compositions, surface and cross-section morphologies and coating thicknesses were determined as a function of the electrode distance. Combined with the simulated current density distribution (analyzed by COMSOL Multiphysics software), the effect of electrode distance on anode current and PEO coating on AM50 magnesium alloy will be discussed.

2. Experimental procedures

2.1. Material and PEO treatment

AM50 magnesium alloy substrates with the composition (mass fraction) of 4.4%–5.5% Al, 0.26%–0.6% Mn, max. 0.22% Zn, max. 0.1% Si, max. 0.002% Fe, max. 0.001% Cu, max. 0.001% Ni and Mg balance were cut into dimensions of 15 mm × 15 mm × 4 mm. Prior to coatings, the substrates were grounded successively by 320, 500, 800, 1200 grit emery sheets and cleaned with ethanol. Then the AM50 substrate and a stainless steel electrode with the dimensions of 50 mm × 50 mm × 4 mm were located face to face and connected to a DC power supply serving as the anode and cathode respectively. The electrolyte was prepared by adding KOH (1 gL-1) and Na3PO4 (10 gL-1) to deionized water. A schematic of the experimental system unit is shown in Fig.1. The electrode distance was adjusted with an accuracy of ± 0,1 mm and the current evolution during PEO process was recorded. The anode surface facing the cathode was defined as front side, and its opposite side was defined as back side. PEO process was carried out under constant voltage of 350 V for 10 min. During the process, a magnetic stirrer was used and a cooling system maintained the electrolyte temperature at 10 ± 1 ℃. Coatings were produced at distances of 10 mm, 20 mm, 40 mm, 60 mm, 80 mm, 100 mm, 120 mm and 240 mm respectively. The current increased rapidly in a few seconds after the voltage was turned on, and then decreased during the rest of the process time while the voltage was kept constant.

2.2. Coating characterization

Scanning electron microscopy (TESCAN Vega3 SB) in the secondary electron (SE) mode was used to examine the coating surface morphologies and cross-sections. X-ray diffraction measurement (XRD) with Cu-Kα radiation was utilized to determine the phase composition of the PEO coatings. Coating thickness was taken from the cross-section SEM micrographs of 500× magnification analysis using Image analysis software analySIS pro 5.0. For each treatment condition, average coating thickness was estimated from 5 coating samples randomly for statistical reasons.

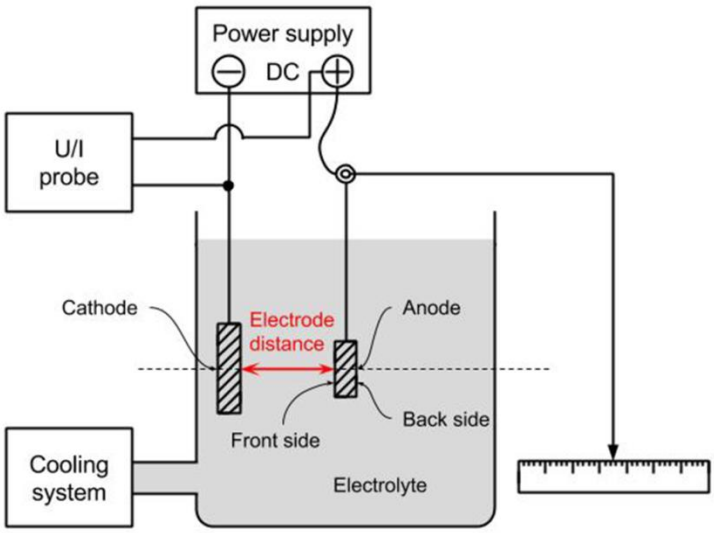

Fig.1 Schematic representation of the experimental set-up.

3. Modelling and simulation

According to the electrochemical principles of PEO process, the physics of secondary current distribution under electrochemistry was chosen to model using the software COMSOL Multiphysics 4.4 software package. The model is stationary which means changing conditions with time is not taken into consideration. Ohm's law is used in combination with a charge balance to describe the conduction of currents in the electrodes and electrolytes. The results of modeling can assist in observation of the current distribution and average current density on the front and back sides of the substrate influenced by varying electrode distances. The electrolyte conductivity measured by a Mettler Toledo Inlab 730 probe was 1.5 S/m. Based on the experimental set-up with model domains consisting of boundaries corresponding to the working electrode, counter electrode, electrolyte, and cell walls, a simplified 2-dimensional model was built with the following assumptions:

i. The substrate and electrolyte is homogeneous and isotropic.
ii. There is no additional external current density or current source.
iii. The concentration gradient is negligible.
iv. Film formation on anode surface has no impact on the current.

According to Ohm's law, the current density *j* at any point in the electrolyte depends on the gradient of local potential φ.

$$j = -\sigma \nabla \varphi \tag{1}$$

where σ is the electrolyte conductivity. By the divergence theorem, the differential form of Gauss's law can be written as:

$$\nabla \cdot E = \frac{\rho}{\varepsilon} = 0 \tag{2}$$

where ∇ · E is the divergence of the electric field, ε is the di-electric constant, and in the electrolyte ρ is the total electric charge density exchange which is 0 (current conservation). So the potential distribution in the electrolyte can be described by the Laplace equation:

$$\nabla^2 \varphi = 0 \tag{3}$$

The boundary conditions for the model are expressed as follows:

1) For all the insulation walls, there is no current flow.

$$-\mathbf{n} \cdot \mathbf{j} = 0 \tag{4}$$

2) The anode is assumed to have a constant applied voltage.
3) The cathode current is expressed by linearized Butler-Volmer kinetics.

$$j_{loc} = j_0 \left(\frac{(\alpha_a + \alpha_c)F}{RT} \right) \eta \quad (5)$$

where R is the universal gas constant, F is Faraday constant, T is temperature, j_0 is the exchange current density, α_a and α_c are anodic and cathodic transfer coefficient, and η is the local potential on the cathode given by equation (6):

$$\eta = \varphi_s - \varphi_l \quad (6)$$

where φ_s is the electric potential on cathode and φ_l is the potential of the solution adjacent to the cathode. With all the conditions and parameters in Table 1, Eq.(3) was numerically solved via finite element method.

The average current density j_{ave} on the front and back sides were determined by the following equation (integration along the boundary elements):

$$j_{ave} = \frac{1}{L} \int_0^L j(y) dy \quad (7)$$

where L is the electrode length on the front or back side.

Table 1: Physical input parameters used in the numerical simulation

Physical parameter	Value
AM50 conductivity (S/m)	4×10^7
Steel conductivity (S/m)	4.032×10^6
Electrolyte conductivity σ (S/m)	1.5
Initial applied voltage on anode (V)	350
Electric potential on cathode φ_s (V)	0
Anodic transfer coefficient α_a	0.5
Cathodic transfer coefficient α_c	0.5
Exchange current density (A/m^2)	10

3.1 Simulation results - Anode current distribution

From the simulation results, information how the current density distributes with different electrode distances on the surfaces of the front sides and back sides of the anodes are presented in Fig.2. For each sample surface, current density distributes non-uniformly which decreases from outside to the center of the substrate surface, and higher current density occurs on the front surface compared to the back surface. On the other hand, both front and back current density decrease with the increasing electrode distance. The difference between them decreases with the electrode distance as well, which indicates that the current density distributes more and more uniformly. Experimental results in Ref. [18] proved that the currents flowing through the front surface is higher than that flowing through the back surface of aluminum alloy and the average current decreases with larger electrode distances, which corresponds to the simulation results.

3.2 Simulation results - Average current density

The dependence of average current density values of the front and back surfaces of the substrates on the electrode distances is displayed in Fig.3. Both the front and back average current density values decrease with larger electrode distances nonlinearly, but the evolution on the front surface is much more evident than that on the back side, especially within short distances up to 80 mm. After 100 mm, the decrease rate of the average current density on both front and back surfaces becomes lower and the current density discrepancy between front and

back surfaces gets smaller. Because of the high electric conductivity of electrodes, the whole system resistance stems mainly from the electrolyte. When the distance is close, the electric

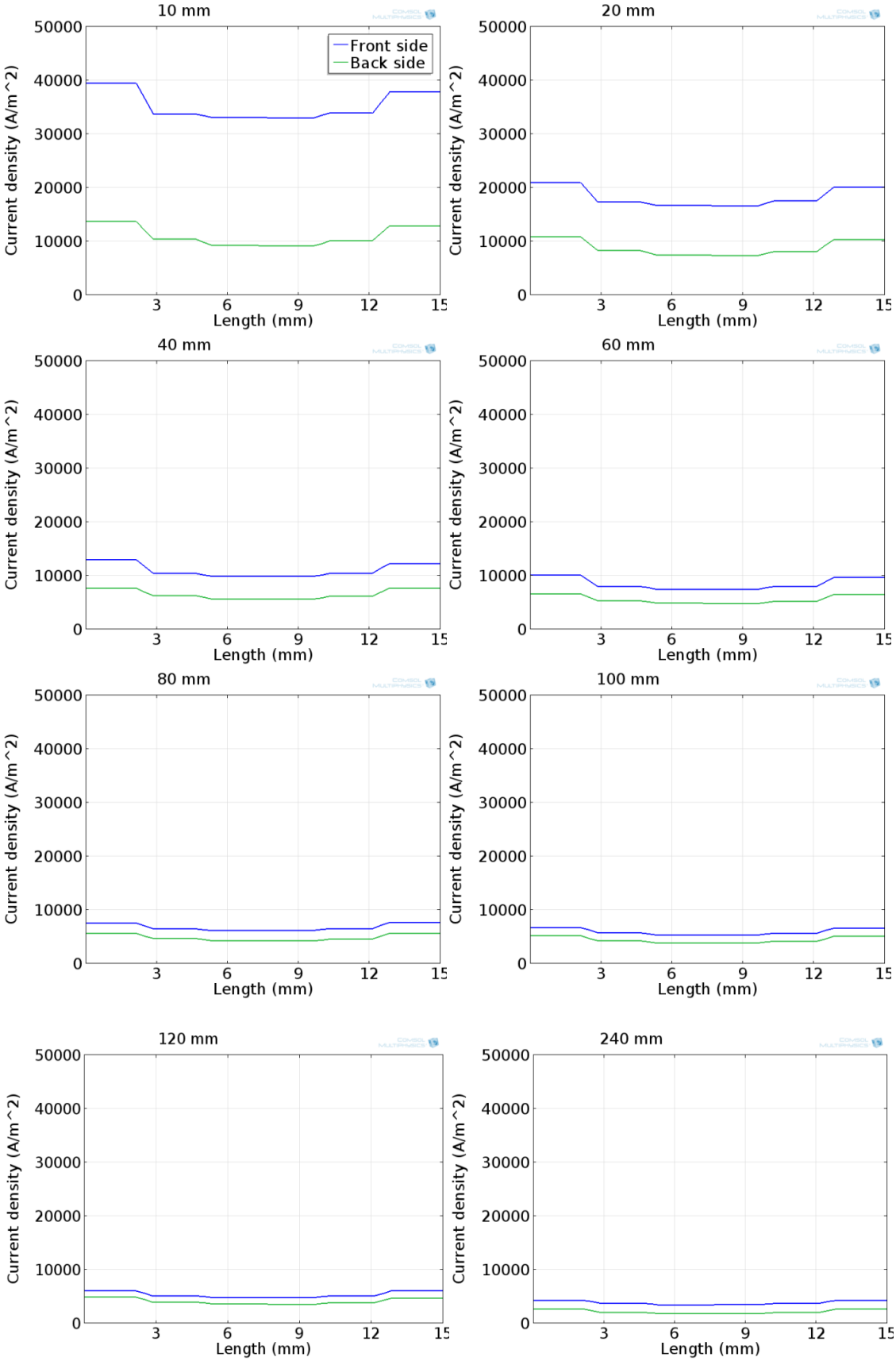

Fig.2 Current density distribution on the surfaces of the front sides and back sides of the anodes for different electrode distances.

field between anode and cathode can be deemed as uniform, so the front anode current decays reciprocally with the electrode distance. When the electrode distance becomes larger, the electric field between anode and cathode becomes non-uniform and thus has a weaker influence on anode current. As for the back side of anode, the electric field is always non-uniform, and due to the shelter effect [18] of the front side, the anode current is lower than that on the front side. So under the constant voltage mode, the average current density is influenced evidently through the distance between anode and cathode.

The simulation results show that electrode distance is an importance factor which affects the initial anode current on both front and back sides, especially at closer distance. The experiment [18] confirmed the same result that current is evidently influenced when the electrode distance is closer, and when the distance becomes larger, it has a weaker influence on anode current.

However, the simulation result just corresponds to the initial current value due to the stationary approach. For the whole PEO process, the experimental evaluation of current is depicted in Fig.4. As can be seen, there is little difference in the current evolution with time resulted from electrode distance except in the first 20 s. The current increases rapidly reaching the summit within a very short period of time about 2 s, and then decreases dynamically within 10 s followed by a relatively slow decline. But, if current reaches the summit then also voltage ramps to 350 V almost at the same time. So the summit current is considered as the initial current, which gets lower when the electrode distance is increasing. By the end of the processing time, the current value drops to approx. 0.02 A for all the coatings. Evidently, the influence of electrode distance on anode current embodies mainly in the initial stage of treatment ($\leq$ 20 s). Afterwards, the influence becomes weaker.

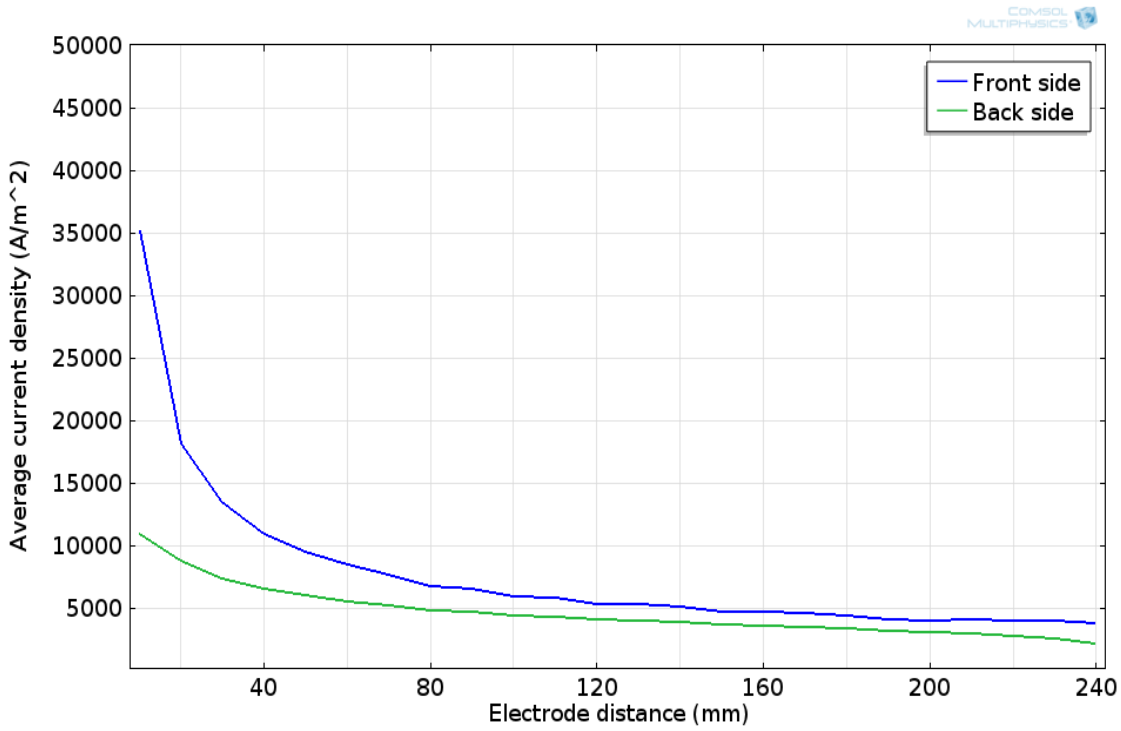

Fig.3 Average current density on the front and back surfaces of the substrates as a function of the electrode distance.

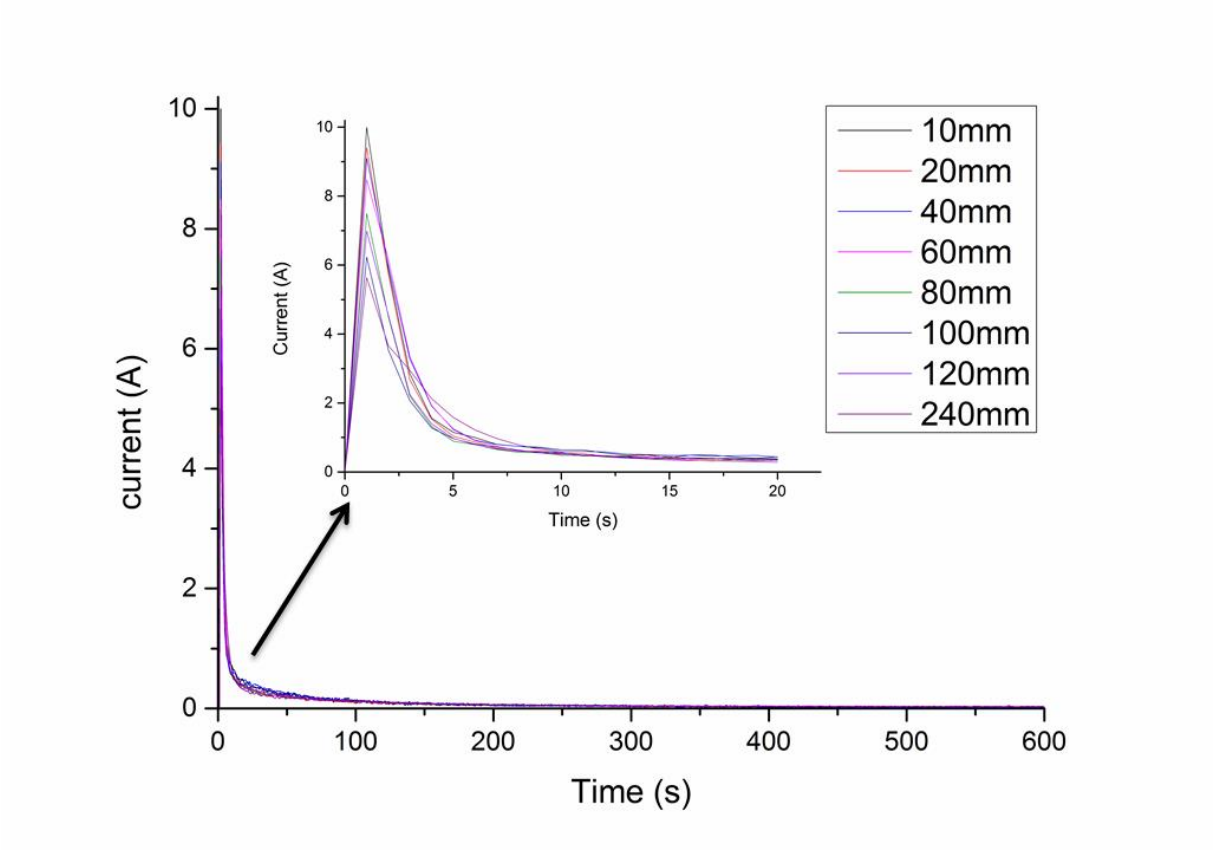

Fig.4 Evolution of current vs. treatment time during the PEO process using constant voltage mode.

4. Experimental results and discussion

4.1 Phase composition

XRD pattern obtained from the eight coatings with different electrode distances in Fig.5 shows little difference. All the coatings exhibit an identical phase composition of magnesium phosphate and magnesium oxide. Considering the same electrolyte components and stirring effect, the electrode distance has no effect on the chemical reaction mechanism of coating formation. Some papers [19,20] claimed that changing the current mode, like using pulsed bipolar current mode, can change the coating composition. Duration and ratio of different stages during PEO process can be altered by the applied electrical process parameters [10], and as a result they influence the number, intensity and energy of the micro-discharges [21] which can determine the thermal and chemical conditions during PEO process, and thus change the phase composition of the coating. Current density is the main source to furnish energy for micro-discharge. In this research, the current density values of the initial stage are altered by electrode distances, but according to Fig.4 this stage lasts obviously too short to change the phase composition. The appearance of Mg peaks is due to the X-ray beam which penetrates entirely the PEO coating and reaches the magnesium substrate. Differences of the ratio of α-Mg peak intensities are related to crystallographic texture effects. The intensity of α-Mg peaks for coating produced at 10 mm distance are the lowest, indicating that the PEO coating produced at 10 mm distance is the thickest.

4.2 Coating morphology

For the front sides of PEO coatings obtained from PEO process with different electrode distances, the SEM morphologies of the free surfaces are displayed in Fig.6 (a-h). Coating with distance of 10 mm presents a rough surface covered by a large portion of thicker coating.

Then the ratio of the thicker fraction decreases with the increase of distance. Electrode distances in the middle range (60 – 80 mm) show nearly perfect and uniform coating surfaces. For distance too remote non-uniform coating growth appears again, but the appearance has changed. The thicker regions appear to be loose and not perfectly sinked, maybe due to less current in the discharges. The polished cross-sections on the front sides of PEO coatings are shown in Fig.7 (a-h). Typically, PEO coating produced from phosphate based electrolytes comprises up to three sub-layers [19], including a dense inner layer, a region with accumulated pores in a form of a pore band and a more compact outer layer penetrated by discharge channels. The inner layers adjacent to the substrates are very thin and displaying wavy-jagged appearance. The outer layers contain irregular pores and discharge channels. Between the two layers elongated pore bands which are orientated parallel to the surface and normally observed when using phosphate based electrolyte and applying a DC mode on magnesium alloy substrates [10,19]. The amount seems to decrease over the electrode distance.

For the back sides of PEO coatings, the free surface morphologies are showing the same trend like the front sides and deliver no further information. SEM performed on polished cross-sections of the back sides of PEO coatings with different electrode distances are shown in Fig.8. The coating thickness is thinner compared to the front side. It is evident that the coating thickness on the front side decreases as the electrode distance increases. However, except the coatings up to 20 mm distance, coating thickness on the back side shows little difference. PEO can produce thicker coatings at closer distances, uniform coatings in the middle range of electrode distances, but thinner and non-uniform coatings at further distances. So adjusting the electrode distance may offer an easy way to improve coating morphology and structure and produce adequate smooth coating.

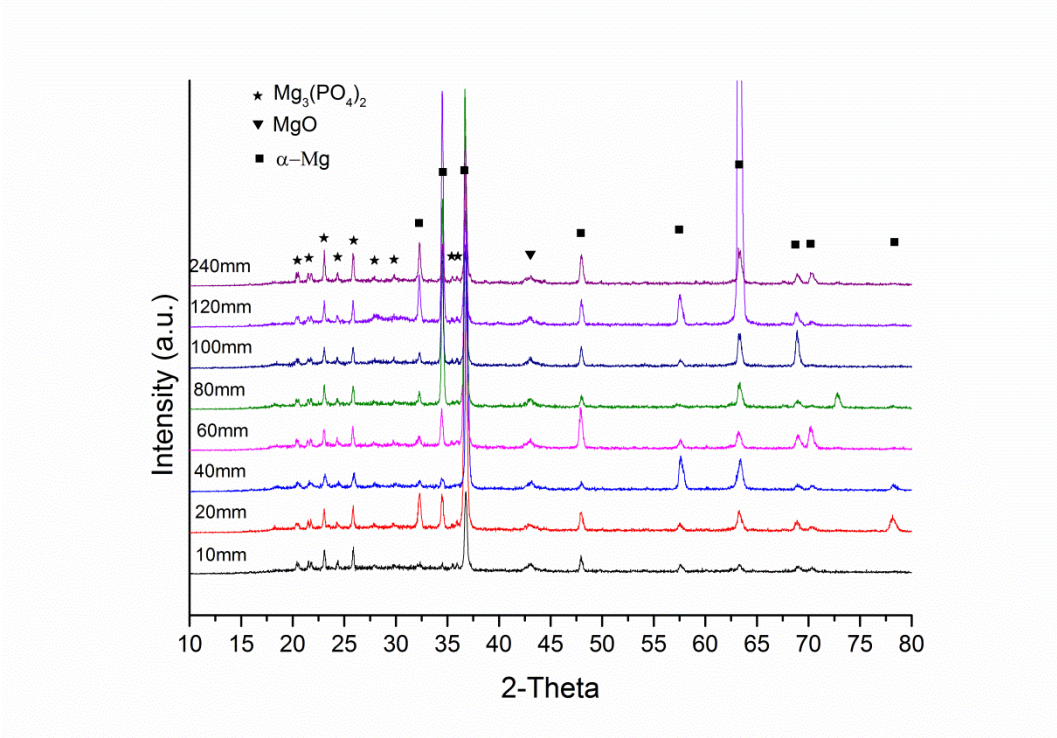

Fig.5 XRD spectra obtained from the eight coatings with different electrode distances.

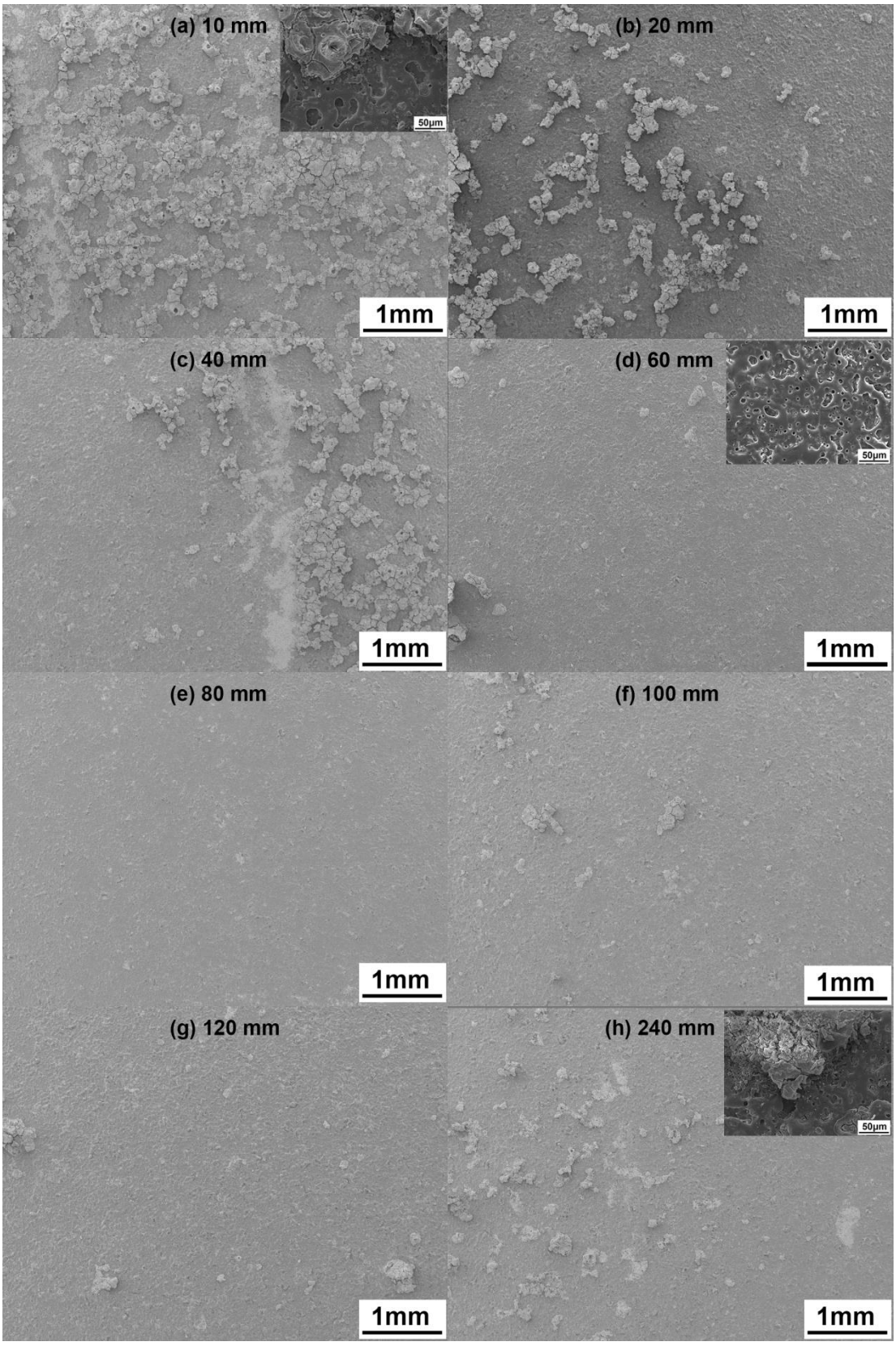

Fig.6 SEM morphologies of free surfaces of the front surfaces of PEO coatings produced with different electrode distances (a) 10 mm, (b) 20 mm, (c) 40 mm, (d) 60 mm, (e) 80 mm, (f) 100 mm, (g) 120 mm, (h) 240 mm.

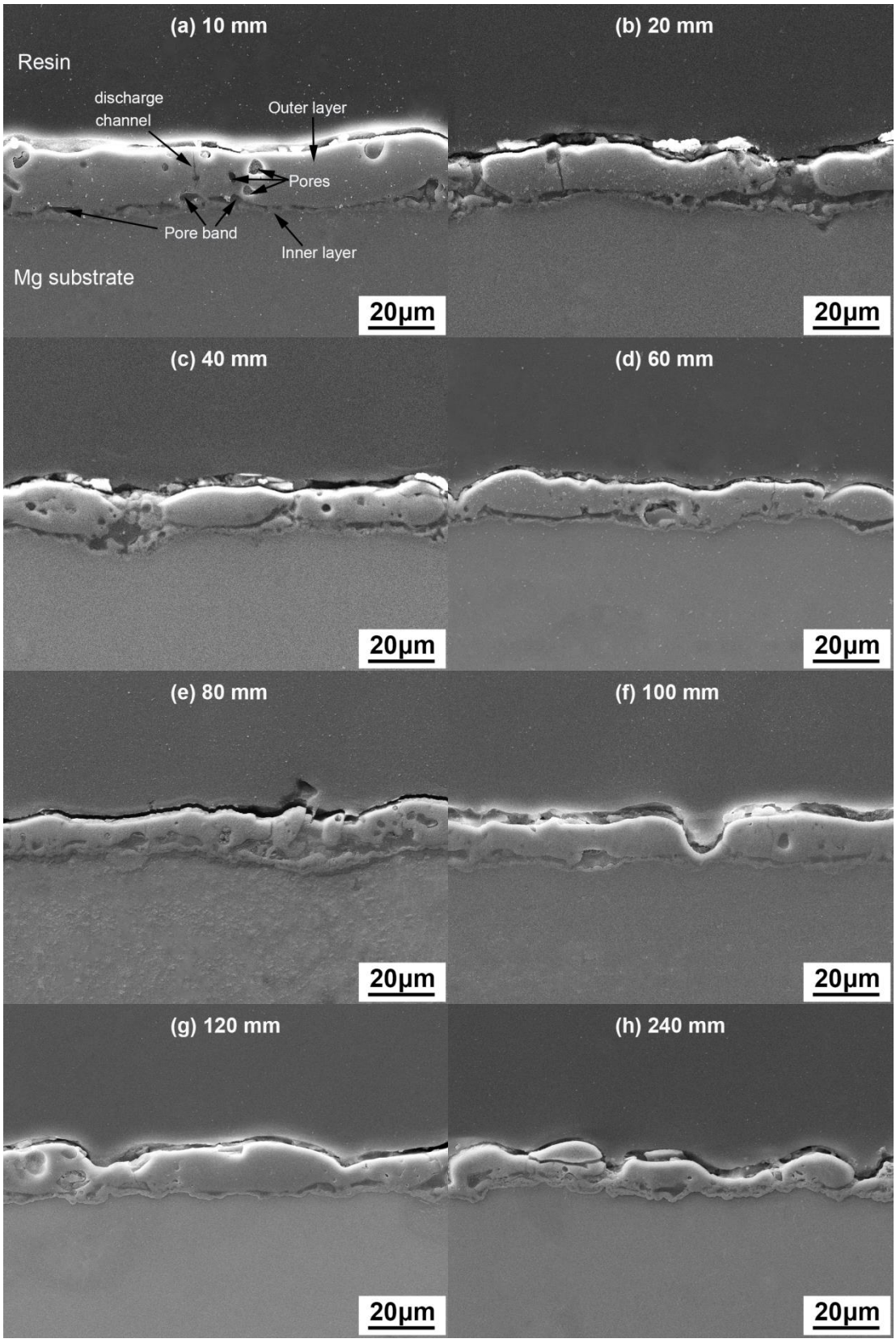

Fig.7 SEM morphologies of the polished cross-sections on the front sides of PEO coatings prepared with different electrode distances.

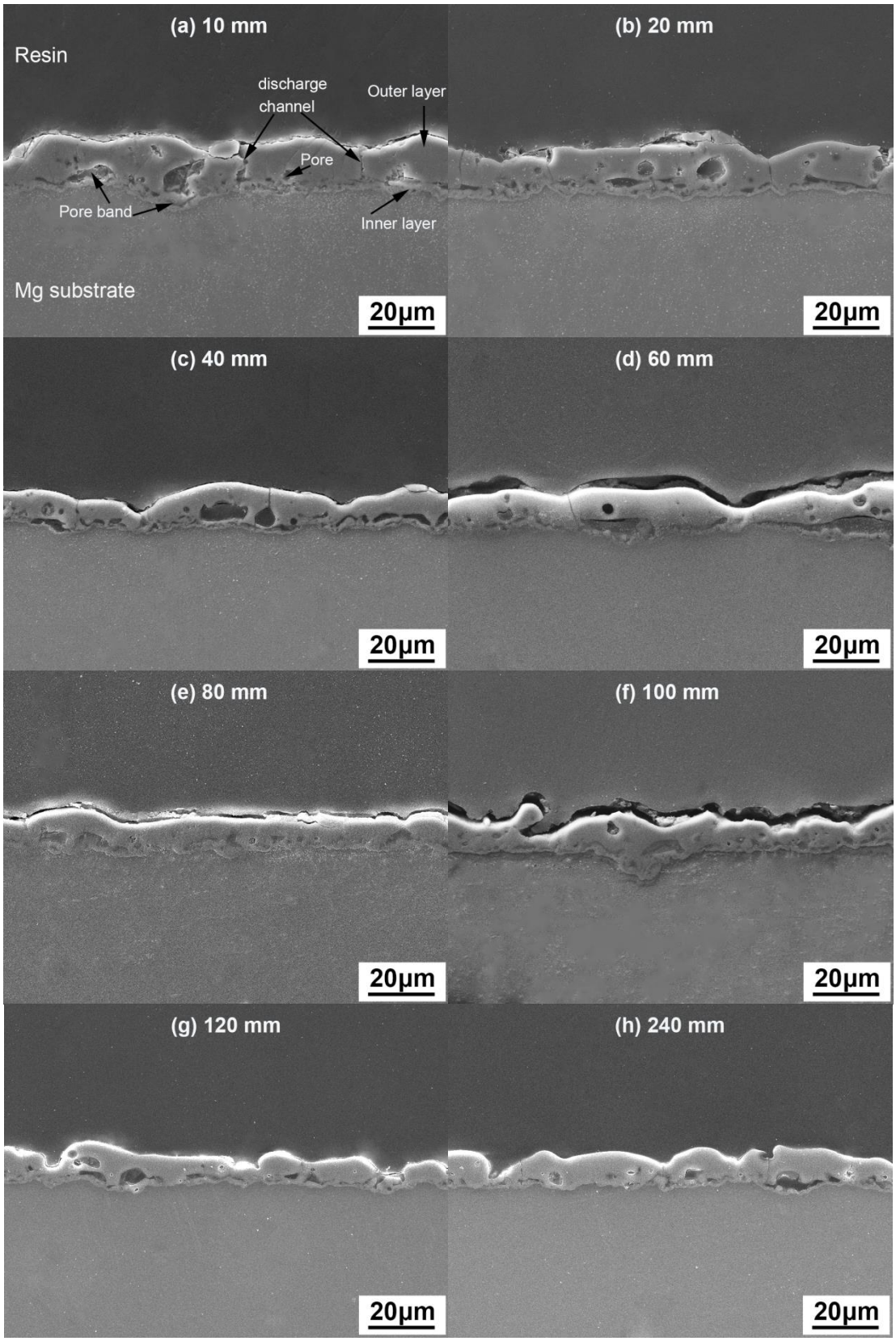

Fig.8 SEM images of the polished cross-sections on the back sides of PEO coatings prepared with different electrode distances.

4.3 Coating thickness

Measured by Analysis pro software package, the evolution of the average coating thickness as a function of electrode distance for the front and back sides of PEO coatings is shown in Fig.9. It is observed that the coating thickness on the front side is higher at each electrode distance compared with the corresponding coating on the back side, and both front and back coating thickness values decrease nonlinearly with the increasing electrode distance. The coating with 10 mm distance has the highest thickness values on both front and back sides which are 23 ± 3 μm and 15 ± 2 μm respectively. Then with the increasing electrode distance, the front thickness decreases significantly, while the back thickness shows much less difference.

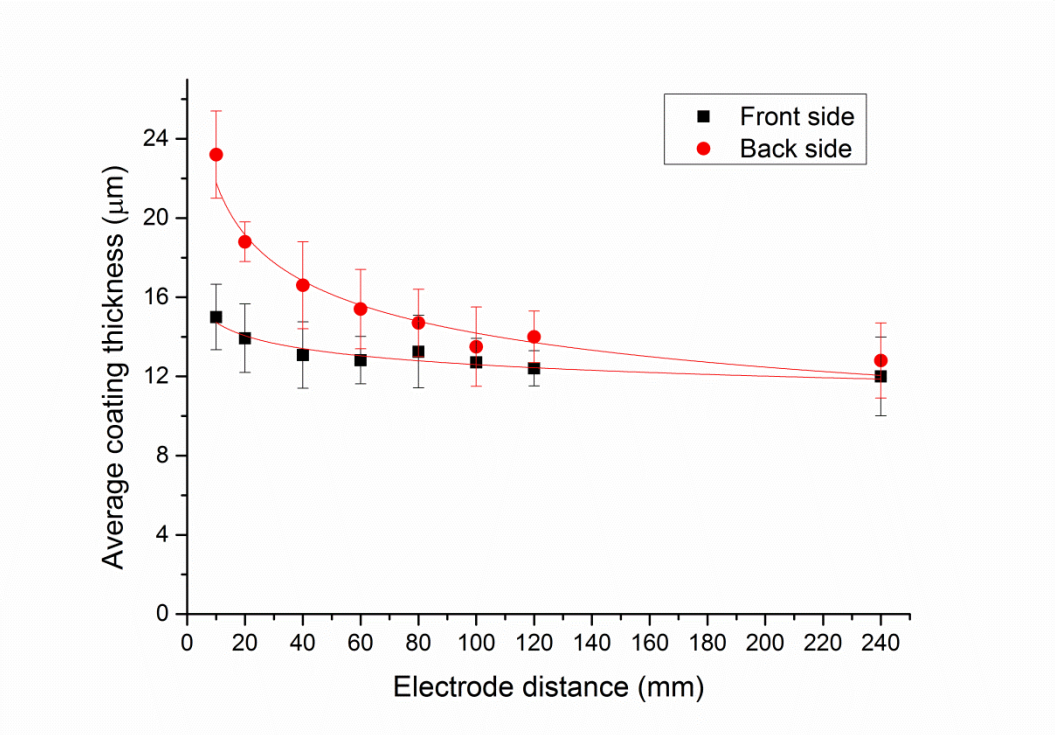

Fig.9 Dependence of the average coating thickness on electrode distance for both the front and back sides of the PEO coatings.

It is well-known that anode current distribution on the whole surface of the specimen has a critical effect on the uniformity of the surface properties and coating thickness [18]. According to the PEO coating formation mechanism [22] proposed before, three main steps lead to PEO coating formation. In the first step, Mg and alloying elements are melted out of the substrate owing to the high temperature generated by electron avalanches, then enter the discharge channel due to the strong electric field, and get oxidized. Second, these oxidized Mg is ejected from the channel into the coating surface in contact with the electrolyte, thereby increasing the coating thickness in that location. In the last step, the discharge channel gets cooled and the reaction products are deposited onto its walls. The above process repeats itself at a number of discrete locations over the entire coating surface, leading to an overall increase in the coating thickness. In accordance with Faraday's laws of electrolysis, coating thickness is proportional to the quantity of electricity transferred at anode. Even though the efficiency of PEO coating formation for magnesium is low due to oxygen generation, dissolution of species in the electrolyte and loss of coating material [23], it is still a common sense that coating thickness grows linearly with the PEO processing time in constant current mode, which could be explained by this formation mechanism [24]. In constant voltage mode, the difference of quantity of electricity resulted from electrode distance is mainly determined by

the initial current. The simulation results of front and back current density as a function of electrode distance show the similar tendency with the coating thickness of front and back sides respectively as a function of electrode distance, indicating that the coating thickness depends mainly on the initial current. Closer distance can reduce the electric quantity loss and result in thicker coating. Therefore, electrode distance is an important factor which can affect coating thickness through changing the current.

5. Conclusions

The simulation results reveal, on the one hand, that current distributes non-uniformly along the substrate surfaces and decrease from the edges to the center. With increasing distance the current gradients from edges to the center get smaller, which means that the current distribution becomes more and more uniform. On the other hand, increasing electrode distances result in nonlinear decline of the average current density at the front and back surfaces of anodes. This also lowers current density differences between them. The simple modelling approach can already be applied to optimize the PEO setup. In order to approach PEO process more realistically, a transient model extension including surface reactions and layer growth would be required.

The experimental results show that surface morphology and coating thickness are influenced by the electrode distance, although there is no influence on the phase composition. The coating on the front side of the sample is thicker than that on the back side of the same sample, and with increasing electrode distances, their experimentally determined thickness evolution show the same tendency with modelled and experimentally measured current density. The results above indicate that the electrode distance can indeed affect the coating characteristics through changing the current distribution and average current density on the front and back surfaces of the sample.

Therefore, we come to the conclusion that the electrode distance is not negligible. In contrast, it is an important factor that can influence PEO coating properties through altering the current distribution and average current density on the surface of treated materials under constant voltage mode.

Acknowledgements

The authors are grateful for funding of the award of fellowship from China Scholarship Council to Xun Ma and the technical assistance of Mr. Ulrich Burmester during the course of this work.

Reference

[1] C.S. Dunleavy, J.A. Curran, T.W. Clyne, *Plasma electrolytic oxidation of aluminium networks to form a metal-cored ceramic composite hybrid material.* Comps. Sci. and Technol., 71 (2011), pp. 908-915.

[2] F. Xu, Y. Xia, G. Li, *The mechanism of PEO process on Al–Si alloys with the bulk primary silicon.* Appl. Surf. Sci., 255 (2009), pp. 9531-9538.

[3] X. Lu, C. Blawert, N. Scharnagl, K.U. Kainer, *Influence of incorporating Si_3N_4 particles into the oxide layer produced by plasma electrolytic oxidation on AM50 Mg alloy on coating morphology and corrosion properties.* J. Magn. Alloys., 1 (2013), pp. 267-274.

[4] M. Mohedano, C. Blawert, M.L. Zheludkevich, *Silicate-based Plasma Electrolytic Oxidation (PEO) coatings with incorporated CeO2 particles on AM50 magnesium alloy.* Mater. Design, 86 (2015), pp. 735-744.

[5] G. Lv, H. Chen, X. Wang, H. Pang, G. Zhang, B. Zou, et al., *Effect of additives on structure and corrosion resistance of plasma electrolytic oxidation coatings on AZ91D magnesium alloy in phosphate based electrolyte.* Surf. Coat. Technol., 205 (2010), pp. S36-S40.

[6] R.O. Hussein, D.O. Northwood, X. Nie, *The effect of processing parameters and substrate composition on the corrosion resistance of plasma electrolytic oxidation (PEO) coated magnesium alloys.* Surf. Coat. Technol., 237 (2013), pp. 357-368.

[7] Y. Cheng, M. Mao, J. Cao, Z. Peng, *Plasma electrolytic oxidation of an Al-Cu-Li alloy in alkaline aluminate electrolytes: A competition between growth and dissolution for the initial ultra-thin films.* Electrochim. Acta, 138 (2014), pp. 417-429.

[8] R.O. Hussein, X. Nie, D.O. Northwood, A. Yerokhin, A. Matthews, *Spectroscopic study of electrolytic plasma and discharging behaviour during the plasma electrolytic oxidation (PEO) process.* J. Phys. D. Appl. Phys., 43 (2010), pp. 105-203.

[9] V. Dehnavi, B. Luan, X. Liu, D.W. Shoesmith, S. Rohani, *Correlation between plasma electrolytic oxidation treatment stages and coating microstructure on aluminum under unipolar pulsed DC mode.* Surf. Coat. Technol., 269 (2015), pp. 91-99.

[10] A.G. Rakoch, A.A. Gladkova, Z. Linn, D.M. Strekalina, *The evidence of cathodic micro-discharges during plasma electrolytic oxidation of light metallic alloys and micro-discharge intensity depending on pH of the electrolyte.* Surf. Coat. Technol., 269(2015), pp. 138-144.

[11] R.O. Hussein, D.O. Northwood, X. Nie, *The influence of pulse timing and current mode on the microstructure and corrosion behaviour of a plasma electrolytic oxidation (PEO) coated AM60B magnesium alloy.* J. Alloys. Compd., 541 (2012), pp. 41-48.

[12] X. Ma, S. Zhu, L. Wang, C. Ji, C. Ren, S. Guan, *Synthesis and properties of a bio-composite coating formed on magnesium alloy by one-step method of micro-arc oxidation.* J. Alloys. Compd., 590 (2014) , pp. 247-253.

[13] S.L. Sinebryukhov, A.S. Gnedenkov, D.V. Mashtalyar, S.V. Gnedenkov, *PEO-coating/substrate interface investigation by localised electrochemical impedance spectroscopy.* Surf. Coat. Technol., 205 (2010), pp. 1697-1701.

[14] A.L. Yerokhin, X. Nie, A. Leyland, A. Matthews, S.J. Dowey, *Plasma electrolysis for surface engineering.* Surf. Coat. Technol., 122 (1999), pp. 73-93.

[15] P.B. Srinivasan, J. Liang, C. Blawert, M. Störmer, W. Dietzel, *Effect of current density on the microstructure and corrosion behaviour of plasma electrolytic oxidation treated AM50 magnesium alloy.* Appl. Surf. Sci., 255 (2009), pp. 4212-4218.

[16] R.O. Hussein, P. Zhang, X. Nie, Y. Xia, D.O. Northwood, *The effect of current mode and discharge type on the corrosion resistance of plasma electrolytic oxidation (PEO) coated magnesium alloy AJ62.* Surf. Coat. Technol., 206 (2011), pp. 1990-1997.

[17] A. Melhem, G. Henrion, T. Czerwiec, J.L. Briançon, T. Duchanoy, F. Brochard, et al., *Changes induced by process parameters in oxide layers grown by the PEO process on Al alloys.* Surf. Coat. Technol., 205(2011), pp. 133-136.

[18] C.B. Wei, X.B. Tian, S.Q. Yang, X.B. Wang, Ricky K.Y. Fu, Paul K. Chu, *Anode current effects in plasma electrolytic oxidation.* Surf. Coat. Technol., 201 (2007), pp. 5021-5024.

[19] Dehnavi, V., X. Liu, B. L. Luan, D.W. Shoesmith, S. Rohani, *Phase transformation in plasma electrolytic oxidation coatings on 6061 aluminum alloy.* Surf. Coat. Technol., 251(2014), pp. 106-114.

[20] Y. Cheng, F. Wu, E. Matykina, P. Skeldon, G.E. Thompson, *The influences of microdischarge types and silicate on the morphologies and phase compositions of plasma electrolytic oxidation coatings on Zircaloy-2.* Corros. Sci. 59 (2012), pp. 307-315.

[21] C. Blawert, S.P. Sah, J. Liang, Y. Huang, D. Höche, *Role of sintering and clay particle additions on coating formation during PEO processing of AM50 magnesium alloy.* Surf. Coat. Technol., 213(2012), pp. 48-58.

[22] G. Sundararajan, L. Rama Krishna, *Mechanisms underlying the formation of thick alumina coatings through the MAO coating technology*. Surf. Coat. Technol., 167(2003), pp. 269-277.

[23] R. Arrabal, E. Matykina, T. Hashimoto, P. Skeldon, G.E. Thompson, *Characterization of AC PEO coatings on magnesium alloys*. Surf. Coat. Technol., 203 (2009), pp. 2207-2220.

[24] R.O. Hussein, X. Nie, D.O. Northwood, *An investigation of ceramic coating growth mechanisms in plasma electrolytic oxidation (PEO) processing.* Electrochim. Acta, 112 (2013) , pp. 111-119.